Scientific Research Publishing

Journal of Power and Energy Engineering, 2026, 14(1), 67-76
https://www.scirp.org/journal/jpee
ISSN Online: 2327-5901
ISSN Print: 2327-588X

Triazine Covalent Organic Framework-Anchored Fe for Efficient Electrocatalytic Oxygen Reduction Reaction

Xue Zhang, Yanfang Gao

Inner Mongolia University of Technology, Hohhot, China
Email: 3142443885@qq.com

How to cite this paper: Zhang, X. and Gao, Y.F. (2026) Triazine Covalent Organic Framework-Anchored Fe for Efficient Electrocatalytic Oxygen Reduction Reaction. *Journal of Power and Energy Engineering*, **14**, 67-76.
https://doi.org/10.4236/jpee.2026.141004

Received: November 14, 2025
Accepted: January 27, 2026
Published: January 30, 2026

Abstract

A nitrogen-rich covalent organic framework material (SNW-1) was prepared via oil bath reflux method. Metal center Fe was introduced by a post-doping strategy, and the Fe-N-SNW-1 catalyst was synthesized through calcination. The electrocatalytic performance of this catalyst for the oxygen reduction reaction (ORR) was investigated. The crystal structure and elemental chemical states of the Fe-N-SNW-1 catalyst were comprehensively characterized by scanning electron microscopy (SEM), X-ray diffraction (XRD), Raman spectroscopy, X-ray photoelectron spectroscopy (XPS) and other techniques. Electrochemical tests including cyclic voltammetry (CV) and linear sweep voltammetry (LSV) were used to explore its ORR electrocatalytic activity. The results show that the Fe-N-SNW-1 catalyst exhibits a microspherical morphology, high graphitic nitrogen content, and excellent ORR electrocatalytic performance. Analysis of key electrochemical parameters indicates that the Fe-N-SNW-1 catalyst has an onset potential of 0.975 V vs. RHE and a half-wave potential of 0.841 V vs. RHE.

Keywords

Fuel Cell, Oxygen Reduction Reaction, Fe-N-SNW-1 Catalyst, Nitrogen-Doped Carbon

1. Introduction

With the rapid development of the global economy and the continuous expansion of the population, humanity's excessive consumption of energy has been intensified. In addition, the severe shortage of fossil energy and its environmental pollution have also prompted people to focus more on exploring alternative new energy

systems [1] [2]. Among a wide range of new energy conversion devices, fuel cells and metal-air batteries have received considerable research attention on account of their relatively higher energy density and power density [3] [4]. However, the sluggish oxygen reduction reaction kinetics at the cathode limits the rapid development of fuel cells and metal-air batteries. The primary reason for this slow kinetics lies in the high bond energy of the O=O bond (498 kJ/mol) [5] [6]. Currently, Pt/C catalysts are widely used in the market [7]. However, their inherent drawbacks—including high cost, scarce reserves, and poor durability—have limited their large-scale application as cathode catalysts in fuel cells and metal-air batteries [8].

Transition metal-nitrogen-carbon (M-N-C) materials have garnered widespread attention due to their low cost, abundant reserves, high selectivity, and ability to provide abundant active sites [9]. However, most transition metal-based catalysts still suffer from inherent drawbacks, such as a limited number of active sites, low exposure degree of active sites, the linear scaling relationship between intermediates, structural instability, and easy dissolution or agglomeration in strong alkaline environments—all of which hinder their further practical applications [10] [11]. In this study, the electrocatalytic activity of ORR is primarily enhanced by increasing the number of active sites and improving the intrinsic activity. The main approach to regulating the number of active sites involves geometric structure modulation [12] [13]. In this study, a porous structured material SNW-1 was synthesized [14] [15]; for the improvement of intrinsic activity, the primary strategy involves regulating the electronic structure [16] [17], and this work adopts heteroatom doping and coordination environment modulation to achieve this goal. Both experimental and theoretical studies have demonstrated that introducing heteroatoms into the carbon framework is a promising strategy, which can modify the electronic state of central metals by altering the charge distribution and spin density of adjacent carbon atoms, thereby enhancing the catalytic activity of the material and optimizing the adsorption of key ORR intermediates [18] [19]. Nitrogen is the most extensively studied heteroatom, attributed to its tunable electronic structure and excellent ORR activity [20].

Among various porous nanomaterials, covalent organic frameworks (COFs), as a new type of porous organic polymer, possess precisely controllable structural motifs connected by covalent bonds [21] [22], COFs exhibit excellent characteristics, such as large specific surface area, high crystallinity, tunable pore size, and unique molecular structure. Owing to these distinctive properties, COFs have been widely applied in the field of catalysis [23]. The large specific surface area, tunable structure, and porous nature of COFs make them ideal candidates for electrocatalysts [24]. At present, substantial progress has been made in the design and synthesis of COFs from low-cost monomer precursors, and COFs have been explored as a supporting material for electrocatalytic oxygen reduction reactions.

Due to the different electronegativities of elements in COFs, the electronic configuration of C can be regulated by adjacent heteroatoms, which in turn induces

changes in its charge density. This endows C-based materials with abundant oxygen adsorption sites and enhanced catalytic performance for ORR [25] [26]. The introduction of metal Fe can form Fe-N_x active sites, which serve as efficient catalytic centers for ORR and significantly reduce the reaction energy barrier [27] [28]. Moreover, Fe doping optimizes the electronic structure of the catalyst, improves electron transfer rate, and minimizes charge loss during the reaction. Additionally, some Fe-based compounds (e.g., Fe_3O_4) possess excellent electrical conductivity and stability, which can enhance the overall reaction kinetics of the catalyst [29] [30].

Based on the above context, the entire workflow of this study involves synthesizing COFs using different types of N-containing ligands, followed by introducing metal ions and forming metal centers through pyrolysis. Owing to the uniform distribution of N atoms in the COF skeleton, efficient N-doping into the carbon matrix can be achieved during the pyrolysis process, which is favorable for the electrocatalytic ORR.

Building on the abovementioned strategy, a two-step method was adopted to synthesize the Fe-N-SNW-1 catalyst with high nitrogen doping content. Firstly, SNW-1 was fabricated via the Schiff base reaction using melamine and terephthalaldehyde as ligands. With $FeCl_3 \cdot 6H_2O$ as the iron source, the abundant N-containing sites in the pores of SNW-1 enabled the adsorption of Fe^{3+} ions into its cavities through electrostatic interaction. Subsequent pyrolysis of the Fe^{3+} adsorbed SNW-1 yielded the Fe-N-SNW-1 catalyst. The results demonstrated that the as-prepared Fe-N-SNW-1 catalyst exhibited a micro-mesoporous morphology, which facilitates the contact between the electrolyte and the catalytic active sites while enhancing the utilization efficiency of the active sites. Furthermore, elemental analysis of the Fe-N-SNW-1 catalyst confirmed a high graphitic N content and the formation of Fe-N bonds. Electrochemical performance tests revealed that the Fe-N-SNW-1 catalyst possessed an onset potential of 0.975 V vs. RHE and a half-wave potential of 0.841 V vs. RHE, indicating excellent electrocatalytic activity for ORR.

2. Experimental Section

2.1. Experimental Materials

Ferric chloride, terephthalaldehyde, and melamine were all of analytical grade and purchased from the Aladdin official website. Acetone, tetrahydrofuran (THF), and dichloromethane were analytical grade reagents acquired from Liano Longbohua Pharmaceutical & Chemical Co., Ltd. Deionized water used in the experiment was self-prepared distilled water in the laboratory.

2.2. Maintaining the Integrity of the Specifications

According to previous literature reports, SNW-1 was synthesized via Schiff base condensation reaction of melamine (MA) and terephthalaldehyde (TA) in anhydrous dimethyl sulfoxide (DMSO) solvent at 180˚C for 72 hours [31]. Specifically, 4.023 g of MA and 2.522 g of TA were weighed and dispersed in 200 mL of DMSO,

followed by ultrasonic dispersion for 30 minutes. Subsequently, the dispersion was transferred into a 500 mL round-bottom flask, and the reaction was conducted at 180 ˚C for 72 hours under a nitrogen (N_2) atmosphere. The obtained product was washed several times with acetone, dichloromethane, and tetrahydrofuran (THF) respectively, and the precipitate was collected by centrifugation. After freeze-drying for 12 hours, SNW-1 was obtained.

Firstly, $FeCl_3 \cdot 6H_2O$ (0.05 mol) was dissolved in 50 mL of deionized water (H_2O). Then, 0.1 g of SNW-1 was added to the above solution, which was ultrasonically dispersed for 30 minutes and magnetically stirred at room temperature for 12 hours. The Fe@SNW-1 precursor was collected by centrifugation, and then mixed with 10 mL of H_2O and 10 mL of aqueous ammonia ($NH_3 \cdot H_2O$). The mixture was transferred into a 50 mL stainless steel autoclave with a polytetrafluoroethylene (PTFE) liner and heated in a blast drying oven at 150˚C for 12 hours for hydrothermal treatment. The product was further washed with deionized water five times and vacuum-dried at 70˚C for 12 hours. Finally, the obtained material was placed in a tube furnace and heated at 800˚C for 3 hours under a N_2 atmosphere to obtain the Fe-N-SNW-1 catalyst.

2.3. Physical Characterization

Scanning electron microscopic (SEM) images and elemental distribution maps were acquired using a FEI Inspect S50 microscope.

Powder X-ray diffraction (XRD) measurements were performed on an XRD-7000 diffractometer (Shimadzu, Japan) with Cu Kα radiation (λ = 1.5406 Å). The diffraction patterns were recorded in the 2θ range of 10˚ - 80˚ at a scanning rate of 10˚/min.

X-ray photoelectron spectroscopy (XPS) analyses were conducted using a Thermo ESCALAB 250 XI spectrometer to determine the elemental composition and chemical states of the as-prepared materials.

Laser micro-Raman spectra were collected on an INVIA REFLEX Raman spectrometer (Renishaw, UK) with a 532 nm laser excitation. The scanning range was typically set from 100 to 4000 cm^{-1}.

Brunauer-Emmett-Teller (BET) [32] specific surface area and pore size distribution analyses were carried out using an Autosorb iQ automatic gas adsorption analyzer (Quantachrome Instruments, USA).

3. Results and Discussion

SNW-1 was synthesized via oil bath reflux, with the preparation process illustrated in **Figure 1**. Subsequently, the Fe-N-SNW-1 catalyst was fabricated through high-temperature calcination and pyrolysis. The morphology of Fe-N-SNW-1 was characterized by scanning electron microscopy (SEM). As presented in **Figure 2(a)** & **Figure 2(b)**, Fe-N-SNW-1 exhibits a microspherical morphology. SEM images (**Figure 2(c)** & **Figure 2(d)**) demonstrate that the as-prepared Fe-N-SNW-1 catalyst is composed of numerous microspheres, constructing a robust 3D framework

structure. Compared with traditional materials, SNW-1 microspheres offer distinct advantages, including enhanced controllability of pore structure, higher exposure rate of active sites, lower density, and larger specific surface area.

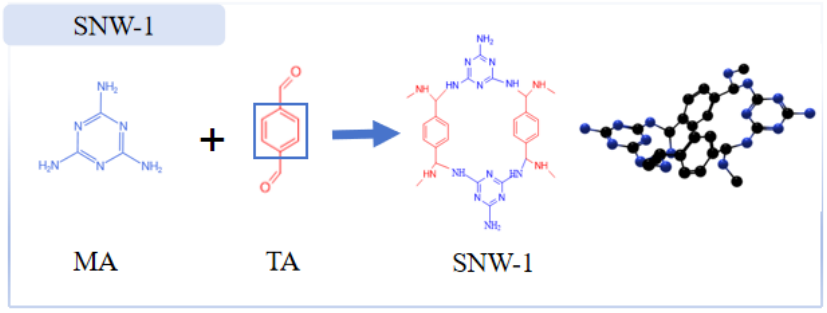

Figure 1. The preparation of SNW-1.

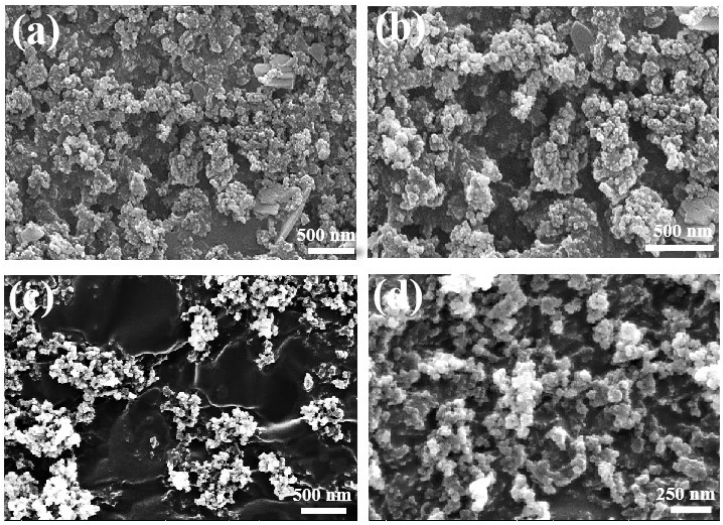

Figure 2. (a), (b) Scanning electron microscopy (SEM) images and schematic diagram of SNW-1; (c), (d) SEM images and schematic diagram of Fe-N-SNW-1.

The synthesis process of SNW-1 was confirmed by Fourier transform infrared (FTIR) spectroscopy. For melamine, the absorption bands at 3471 and 3421 cm^{-1} are attributed to the stretching vibrations of H-N-H, with a bending vibration of H-N-H observed at 1650 cm^{-1}. For terephthalaldehyde, the absorption bands at 1691 and 2870 cm^{-1} correspond to the stretching vibrations of C=O and C-H, respectively. In the synthesized SNW-1, the absorption bands at 3471, 3421, 1691, and 1650 cm^{-1} completely disappeared, indicating the completion of the condensation reaction between the amino groups in melamine and the carbonyl groups in terephthalaldehyde. In contrast, the newly emerged absorption bands at 1558 and 1483 cm^{-1} in SNW-1 are assigned to the quadrant and semicircle stretching vibrations of the triazine ring, respectively, confirming that melamine was successfully incorporated into the SNW-1 framework. No characteristic absorption peak was detected around 1610 cm^{-1}, suggesting that no imine bonds (C=N) were

generated during the condensation reaction. Additionally, the structure of secondary amino groups was confirmed by two absorption bands: the N-H stretching vibration at 3388 cm^{-1} and the C-N stretching vibration at 821 cm^{-1}. The successful synthesis of SNW-1 was also verified by X-ray diffraction (XRD) measurements. In the XRD pattern of Fe-N-SNW-1 (**Figure 3**), two broad and intense peaks at $2\theta = 25^{\circ}$ and 43˚ are assigned to the (002) and (110) crystal planes of amorphous carbon, respectively. No peaks corresponding to metallic Fe were observed. Inductively coupled plasma (ICP) analysis was subsequently performed, revealing an Fe content of 0.132%, which confirms the successful introduction of Fe. The successful incorporation of Fe was further validated by XPS characterization.

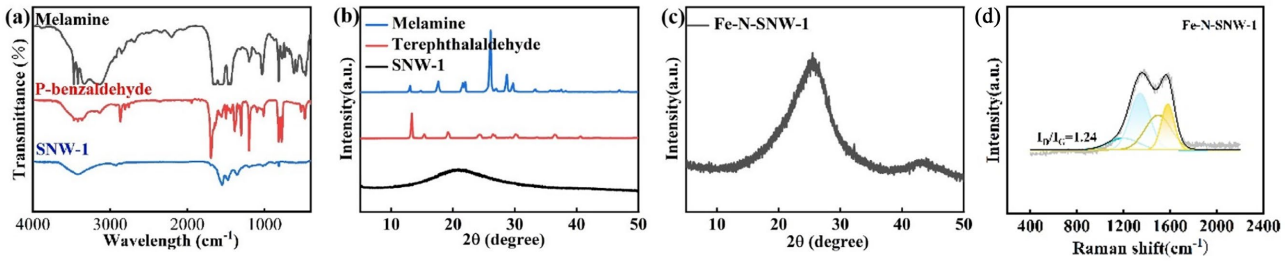

Figure 3. (a) FTIR patterns of P-phthaladehyde, Melamine, SNW-1; (b) XRD patterns of P-phthaladehyde, Melamine, SNW-1; (c) XRD patterns of Fe-N-SNW-1; (d) Raman patterns of Fe-N-SNW-1.

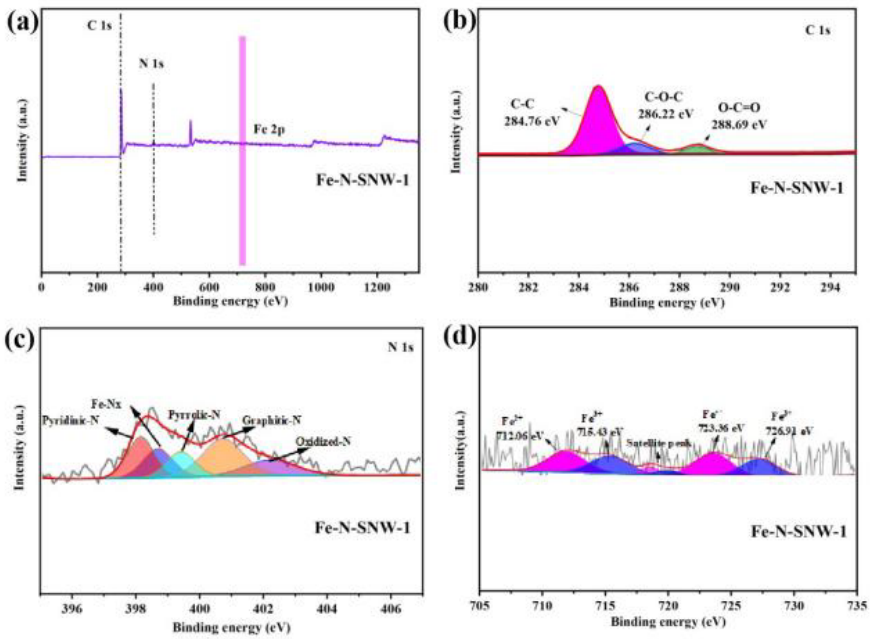

Figure 4. (a)XPS survey spectra of Fe-N-SNW-1; (b) C 1s; (c)N 1s; (d) Fe 2p.

Raman spectroscopic analysis (**Figure 4(d)**) indicates that the intensity ratio of the D band (1350 cm^{-1}) to the G band (1580 cm^{-1}) (I_D/I_G) of Fe-N-SNW-1 is 1.24, suggesting that Fe-N-SNW-1 possesses a moderate defect structure and degree of graphitization. X-ray photoelectron spectroscopy (XPS) was employed to investigate the surface chemical states and structural composition of Fe-N-SNW-1

(**Figure 4**). The high-resolution Fe 2p spectrum (**Figure 3(d)**) exhibits characteristic peaks corresponding to Fe^{2+}, Fe^{3+}, and satellite peaks. The doped N is mainly present in the forms of pyridinic-N, Fe-N_x, pyrrolic-N, graphitic-N, and oxidized-N.

The electrochemical performance of Fe-N-SNW-1 was evaluated using a rotating disk electrode (RDE) and compared with that of the SNW-1 catalyst, as shown in **Figure 5**. The results demonstrate that the as-prepared Fe-N-SNW-1 ORR catalytic performance. Specifically, the catalytic activity of Fe-N-SNW-1 was assessed via cyclic voltammetry (CV) and linear sweep voltammetry (LSV) measurements in a three-electrode system using the RDE.

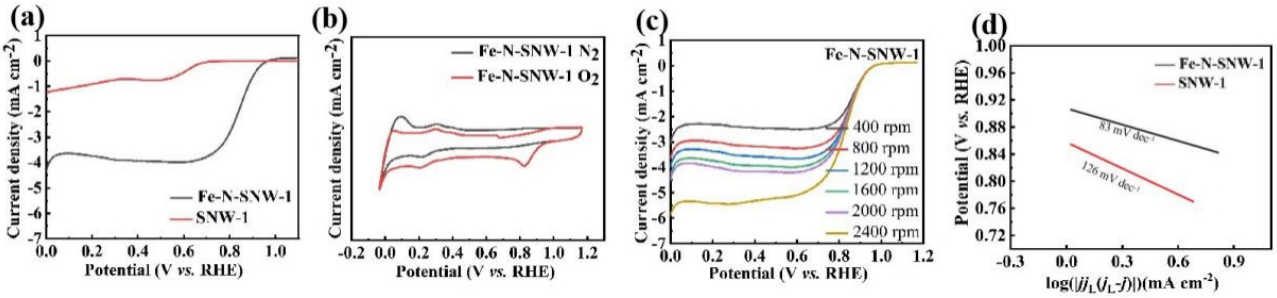

Figure 5. (a) ORR LSV curves of different catalysts; (d) CV curves of Fe-N-SNW-1 in both N_2- and O_2-saturated 0.1 M KOH solution; (c) ORR LSV curves of Fe-N-SNW-1; (d) Tafel slopes.

In **Figure 5(b)**, cyclic voltammetry (CV) curves of Fe-N-SNW-1 were recorded in $N_2$and O_2 saturated 0.1 mol/L KOH electrolytes at a scan rate of 50 mV/s. A distinct cathodic reduction peak is observed in the CV curve obtained in the O_2-saturated electrolyte, indicating that Fe-N-SNW-1 exhibits excellent oxygen reduction reaction (ORR) catalytic activity. To further investigate the reaction kinetics of the Fe-N-SNW-1 catalyst, linear sweep voltammetry (LSV) measurements at different rotation speeds were performed in an O_2 saturated electrolyte (**Figure 5(c)**. The Tafel slope is calculated to be 83 mV dec^{-1}, suggesting a fast kinetic process. This result further confirms that the prepared metal-support catalyst is favorable for accelerating the ORR kinetic process.

4. Conclusions

The as-prepared catalyst exhibits excellent oxygen reduction reaction (ORR) performance, which can be attributed to the following two aspects:

1) The formation of Fe-N species and high graphitic N content provide abundant efficient active sites for the ORR process.

2) The strong interaction between metallic Fe and the SNW-1 support not only generates additional active sites but also facilitates the efficient mass transfer of reactants, intermediates, and products.

Acknowledgements

2025 Autonomous Region University Basic Scientific Research Business Expenses

Project - Inner Mongolia University of Technology: Improving Basic Scientific Research Capabilities of Outstanding On-Campus Students (Graduate School). Project Number: ZTY2025015.

Conflicts of Interest

The authors declare no conflicts of interest regarding the publication of this paper.

References

[1] Ferrandon, M., Kropf, A.J., Myers, D.J., Artyushkova, K., Kramm, U., Bogdanoff, P., *et al.* (2012) Multitechnique Characterization of a Polyaniline-Iron-Carbon Oxygen Reduction Catalyst. *The Journal of Physical Chemistry C*, **116**, 16001-16013. https://doi.org/10.1021/jp302396g

[2] Guo, Y., Wang, Z., Wang, Y., Ma, L., Zhang, N. and Jiang, R. (2022) Efficient Oxygen Reduction Electrocatalyst Derived from Facile Fe,N-Surface Treatment of Carbon Black. *Journal of Colloid and Interface Science*, **605**, 101-109. https://doi.org/10.1016/j.jcis.2021.07.071

[3] Hao, Y., Wang, L. and Huang, L. (2023) Lanthanide-Doped MoS_2 with Enhanced Oxygen Reduction Activity and Biperiodic Chemical Trends. *Nature Communications*, **14**, Article No. 3256. https://doi.org/10.1038/s41467-023-39100-5

[4] Wang, Q., Chen, Z., Wu, N., Wang, B., He, W., Lei, Y., *et al.* (2017) N-Doped 3D Carbon Aerogel with Trace Fe as an Efficient Catalyst for the Oxygen Reduction Reaction. *ChemElectroChem*, **4**, 514-520. https://doi.org/10.1002/celc.201600799

[5] Bhoyate, S.D., Kim, J., de Souza, F.M., Lin, J., Lee, E., Kumar, A., *et al.* (2023) Science and Engineering for Non-Noble-Metal-Based Electrocatalysts to Boost Their ORR Performance: A Critical Review. *Coordination Chemistry Reviews*, **474**, Article ID: 214854. https://doi.org/10.1016/j.ccr.2022.214854

[6] Musgrave, C.B., Su, J., Xiong, P., Song, Y., Huang, L., Liu, Y., *et al.* (2025) Molecular Strain Accelerates Electron Transfer for Enhanced Oxygen Reduction. *Journal of the American Chemical Society*, **147**, 3786-3795. https://doi.org/10.1021/jacs.4c16637

[7] Yamazaki, S., Asahi, M., Taguchi, N. and Ioroi, T. (2019) Electrochemical Analysis of the Porphyrazine-Induced Enhancement of ORR Activity of Pt Catalysts for the Development of Porphyrazine-Adsorbed Pt Catalysts. *Journal of Electroanalytical Chemistry*, **848**, Article ID: 113321. https://doi.org/10.1016/j.jelechem.2019.113321

[8] Qian, Y., Khan, I.A. and Zhao, D. (2017) Electrocatalysts Derived from Metal-Organic Frameworks for Oxygen Reduction and Evolution Reactions in Aqueous Media. *Small*, **13**, Article ID: 1701143. https://doi.org/10.1002/smll.201701143

[9] Zhang, Y. and Guo, Z. (2023) Transition Metal Compounds: From Properties, Applications to Wettability Regulation. *Advances in Colloid and Interface Science*, **321**, Article ID: 103027. https://doi.org/10.1016/j.cis.2023.103027

[10] Wang, Y., Li, J. and Wei, Z. (2018) Transition-Metal-Oxide-Based Catalysts for the Oxygen Reduction Reaction. *Journal of Materials Chemistry A*, **6**, 8194-8209. https://doi.org/10.1039/c8ta01321g

[11] Araújo, H., Šljukić, B., Gago, S. and Santos, D.M.F. (2024) The Current State of Transition Metal-Based Electrocatalysts (Oxides, Alloys, POMs, and MOFs) for Oxygen Reduction, Oxygen Evolution, and Hydrogen Evolution Reactions. *Frontiers in Energy Research*, **12**, Article ID: 1373522. https://doi.org/10.3389/fenrg.2024.1373522

[12] Shen, Y., Li, B., Zhang, Z., Liu, J., Ren, H., Zhou, Y., *et al.* (2025) Selective Adsorption-

Catalytic Action of Spinel Sulfur Reduction Catalyst Based on Geometric Structure Regulation on Lithium Polysulfide. *Electrochimica Acta*, **541**, Article ID: 147345. https://doi.org/10.1016/j.electacta.2025.147345

[13] Xiao, L., Qi, L., Sun, J., Husile, A., Zhang, S., Wang, Z., *et al.* (2024) Structural Regulation of Covalent Organic Frameworks for Advanced Electrocatalysis. *Nano Energy*, **120**, Article ID: 109155. https://doi.org/10.1016/j.nanoen.2023.109155

[14] Samarasinghe, S.A.S.C., Chuah, C.Y., Li, W., Sethunga, G.S.M.D.P., Wang, R. and Bae, T. (2019) Incorporation of Coiii Acetylacetonate and SNW-1 Nanoparticles to Tailor O_2/N_2 Separation Performance of Mixed-Matrix Membrane. *Separation and Purification Technology*, **223**, 133-141. https://doi.org/10.1016/j.seppur.2019.04.075

[15] Vatanpour, V., Tuncay, G., Teber, O.O., Paziresh, S., Tavajohi, N. and Koyuncu, İ. (2024) Introducing the SNW-1 Covalent Organic Framework to the Polyamide Layer of the TFC-RO Membrane with Enhanced Permeability and Desalination Performance. *ACS Applied Materials & Interfaces*, **16**, 65194-65210. https://doi.org/10.1021/acsami.4c14923

[16] Qu, X., Li, Y., Li, G., Ji, R., Yin, S., Cheng, X., *et al.* (2022) Boosting the ORR Performance of Fe-N/C Catalyst via Increasing the Density and Modifying the Electronic Structure of Fe-N_x Active Sites. *Electrochimica Acta*, **403**, Article ID: 139604. https://doi.org/10.1016/j.electacta.2021.139604

[17] Wei, X., Cao, S., Cheng, S., Lu, C., Chen, X., Lu, X., *et al.* (2025) Heterometallic Doping Regulation in Two-Dimensional Metal-organic Frameworks for Enhanced Electrocatalytic Oxygen Reduction Reaction: A Computational Study. *Applied Surface Science*, **713**, Article ID: 164331. https://doi.org/10.1016/j.apsusc.2025.164331

[18] Cheng, J., Lyu, C., Chen, H., Geng, D. and Zheng, J. (2024) Strong Lewis Acid-Base Interfacial Regulation Mechanism to Reveal Oxygen Reduction Activity Origin of N,S-Codoped Carbon with PtNi Particles. *Chemical Engineering Journal*, **482**, Article ID: 149070. https://doi.org/10.1016/j.cej.2024.149070

[19] Li, X., Wang, D., Xu, H., Zha, S., Wang, W., Mitsuzaki, N., *et al.* (2025) Graphitic N-C-P Configuration of Phosphorus and Nitrogen Co-Doped Carbon for Boosting the Oxygen Electroreduction. *Applied Surface Science*, **683**, Article ID: 161814. https://doi.org/10.1016/j.apsusc.2024.161814

[20] Yuan, H., Liu, P., Ren, J., Jiang, Z., Wang, X. and Zhao, H. (2024) Carbon Dot Hybrid Porous Carbon Nanofibers as Efficient Electrocatalysts for the Oxygen Reduction Reaction. *Materials Chemistry Frontiers*, **8**, 1643-1650. https://doi.org/10.1039/d3qm01064c

[21] Malik, H. and Nadeem, M.A. (2025) Unlocking the Two Electron ORR: Synergistic Roles of MOFs and COFs in Mechanistic Insights and Performance Optimization. *Coordination Chemistry Reviews*, **544**, Article ID: 216977. https://doi.org/10.1016/j.ccr.2025.216977

[22] Li, C., Wang, Z., Jin, Y., Li, Z., Jeon, J., Zhao, S., *et al.* (2025) Tunable Catalytic Vertex Wall Chemistry in Metal-Free Covalent Organic Frameworks for Enhanced Oxygen Reduction. *Angewandte Chemie International Edition*, **64**, e202500336. https://doi.org/10.1002/anie.202500336

[23] Du, L., Li, X., Lu, X. and Guo, Y. (2024) The Synthesis Strategies of Covalent Organic Frameworks and Advances in Their Application for Adsorption of Heavy Metal and Radionuclide. *Science of the Total Environment*, **939**, Article ID: 173478. https://doi.org/10.1016/j.scitotenv.2024.173478

[24] Ma, Y., Kuang, X., Deng, X., Zi, B., Zeng, J., Zhang, J., *et al.* (2022) The Recent Research Progress and Application of Nanoparticles and Ions Supporting by Covalent

Organic Frameworks. *Microporous and Mesoporous Materials*, **335**, Article ID: 111701. https://doi.org/10.1016/j.micromeso.2022.111701

[25] Lee, E., Shin, S., Lee, H. and Ham, H.C. (2025) Role of Pz Band in Hybrid Carbon-Bimetallic Subnanocluster PtM (M = 3d, 4d, 5d Block Metals) Catalysts to Boost Electrochemical Oxygen Reduction Reaction. *Applied Surface Science Advances*, **28**, Article ID: 100792. https://doi.org/10.1016/j.apsadv.2025.100792

[26] Li, M.-Y., Liu, J., Gao, R., Lin, D.-Y., Wang, F. and Zhang, J. (2021) Design and Synthesis of Zeolitic Tetrazolate-Imidazolate Frameworks. *Materials Today Advances*, **10**, Article ID: 100145. https://doi.org/10.1016/j.mtadv.2021.100145

[27] Kim, D., Nguyen, A.N. and Yoo, H. (2025) Iron Doping of Coordination Polymer Nanocubes and Post-Thermolysis for Efficient Oxygen Reduction Reaction Single-Atom Catalysis. *Journal of Power Sources*, **641**, Article ID: 236812. https://doi.org/10.1016/j.jpowsour.2025.236812

[28] Gan, R., Wang, Y., Zhang, X., Song, Y., Shi, J. and Ma, C. (2023) Edge Atomic Fe Sites Decorated Porous Graphitic Carbon as an Efficient Bifunctional Oxygen Catalyst for Zinc-Air Batteries. *Journal of Energy Chemistry*, **83**, 602-611. https://doi.org/10.1016/j.jechem.2023.03.056

[29] Fang, L., Li, Y., Zhang, M., Qiu, H., Geng, H., Tao, Y., *et al.* (2024) Anchored Fe_3O_4/Fe Nanoparticles on Hollow PPy Nanotube@Fe-Modified ZIF-8 Derivative for Enhanced ORR Activity in Zinc-Air Batteries. *Diamond and Related Materials*, **149**, Article ID: 111621. https://doi.org/10.1016/j.diamond.2024.111621

[30] Qi, J., Wang, W., Li, Y., Sun, Y., Wu, Z., Bao, K., *et al.* (2022) On-Chip Investigation of Electrocatalytic Oxygen Reduction Reaction of 2D Materials. *Small*, **18**, Article ID: 2204010. https://doi.org/10.1002/smll.202204010

[31] Geng, K., He, T., Liu, R., Dalapati, S., Tan, K.T., Li, Z., *et al.* (2020) Covalent Organic Frameworks: Design, Synthesis, and Functions. *Chemical Reviews*, **120**, 8814-8933. https://doi.org/10.1021/acs.chemrev.9b00550

[32] Williams, J.H., Gbadomosi, M., Greytak, A.B. and Myrick, M.L. (2023) Measuring the Surface Area of Carbon Black Using BET Isotherms: An Experiment in Physical Chemistry. *Journal of Chemical Education*, **100**, 4838-4844. https://doi.org/10.1021/acs.jchemed.3c00764